ACS APPLIED MATERIALS & INTERFACES

Research Article

www.acsami.org

Enhancing the Energy Density of Asymmetric Stretchable Supercapacitor Based on Wrinkled CNT@MnO_2 Cathode and CNT@polypyrrole Anode

Qianqiu Tang, Mingming Chen, Chongyang Yang, Wenqiang Wang, Hua Bao, and Gengchao Wang*

Shanghai Key Laboratory of Advanced Polymeric Materials, School of Materials Science and Engineering, Key Laboratory for Ultrafine Materials of Ministry of Education, East China University of Science and Technology, Shanghai 200237, P. R. China

Supporting Information

ABSTRACT: With the advantages of high stickiness and stretchability of the hydrogel electrolyte as well as the resilient properties of film electrodes, the facile "prestrain-stick-release" strategy can be utilized for the assembly of a stretchable supercapacitor. Two major issues of concern are the relatively low mechanical strength of the hydrogel electrolyte and the low energy density of the assembled device. Herein, vinyl group grafted silica (CH_2═CH—SiO_2) nanoparticles were used as a nanoparticle cross-linker for polyacrylamide (PAAM), enhancing the tensile strength of 844 kPa at the strain of 3400% for the KCl—CH_2═CH—SiO_2/PAAM hydrogel electrolyte. Besides, carbon nanotube supported polypyrrole (CNT@PPy) and manganese dioxide (CNT@MnO_2) film electrodes are prepared to assemble the stretchable asymmetric CNT@MnO_2//KCl—CH_2═CH—SiO_2/PAAM//CNT@PPy supercapacitor, significantly enhancing the potential window to 0−2.0 V and achieving a high energy density of 40 Wh kg^{-1} at the power density of 519 kW kg^{-1} with the strain of 100%, which is the best known for the reported stretchable supercapacitors.

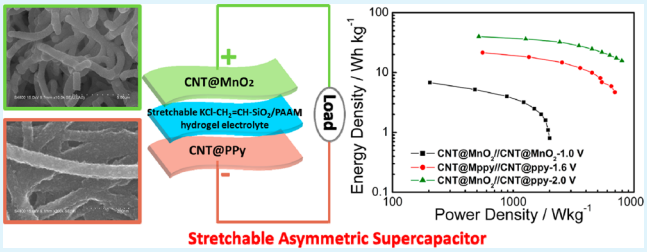

KEYWORDS: *stretchable asymmetric supercapacitor, stretchable hydrogel electrolyte, wrinkled electrodes, polypyrrole, manganese dioxide*

INTRODUCTION

In the past several years, flexible/bendable energy storage and conversion devices (ESCDs) are of great research interest with the rapid development of consumer electronics, such as wearable electronics, electronic papers, mobile phones, and other collapsible gadgets.[1−5] However, flexibility/bendability is far from enough when the scope of research has further expanded to more attractive and technically challenging applications, such as biointegrated devices, space satellites, electric vehicles, and even buildings with arbitrarily shaped surfaces, which often induce strains far exceeding 1%. It explains why stretchable devices, which can undertake not only bending but also compressing, stretching, twisting, and others, have become an emerging research area more recently and may yield mainstream technologies in the near future.[6−12] Among the various forms of ESCDs including batteries[13−17] and solar cells,[18−22] supercapacitors[11,23,24] show great potential for practical application with their obvious advantages such as excellent power performance, cycling life, and safety. Thus, the stretchable supercapacitor has sprung up in the just few years.[7−11]

A fully stretchable supercapacitor device is commonly made up of a stretchable solid electrolyte[25] (functioning as both the electrolyte and separator) sandwiched by two electrodes. Previous reports for stretchable supercapacitors indicate that they often rely on a stretchable rubber base such as polydimethylsiloxane (PDMS)[26] to provide stretchability or involve depositing electrochemically active materials on the stretchable electrolyte preplated with a conductive base of gold.[12] However, both require a complicated assembly process. Recently, we developed a facile "prestrain-stick-release" strategy to assemble a stretchable supercapacitor, which utilizes a highly stretchable and sticky Na_2SO_4-anionic polyurethane acrylates/polyacrylamide (Na_2SO_4-*a*PUA/PAAM) hydrogel electrolyte as stretchable base, thus greatly simplifying the assembly process and improving the mechanical performance of the device.[7] Besides, the strong stickiness of the hydrogel electrolyte ensures its close interface contact with the CNT@MnO_2 film electrodes. However, there are still several major issues which need to be better dealt with regarding the assembly of stretchable supercapcitors so as to enhance the mechanical and electrochemical performance.

First, in a comparison with traditional supercapacitors with liquid electrolyte, the electrochemical performance of the assembled stretchable device needs to be further enhanced. For example, the highest energy density of the reported stretchable

Received: April 12, 2015
Accepted: June 29, 2015
Published: June 29, 2015

DOI: 10.1021/acsami.5b03148
ACS Appl. Mater. Interfaces 2015, 7, 15303−15313

supercapacitor is 15.7 Wh kg^{-1} with the use of an ionic-liquid-based nonvolatile gel (ion-gel) electrolyte.[9] However, it is still far behind the 10−200 Wh kg^{-1} of traditional supercapacitors.[27−29] Assembling asymmetric supercapacitors with different cathodes and anodes is an effective method to broaden the operating potential window, showing great promise for high energy density applications.[30−33] For example, Liu et al. reported an asymmetric supercapacitor with MnO_2/graphene/CNT cathode and polypyrrole/graphene/CNT anode with a broad potential window of 1.6 V, delivering high energy/power density.[33] Thus, it can be anticipated that enhanced electrochemical performance can be achieved by assembling a stretchable asymmetric supercapacitor based on hydrogel electrolyte. Besides, in this case, it avoids the use of expensive ion-gel electrolyte,[9] reducing the cost and facilitating the assembly as well.

Second, as a significant component of stretchable supercapacitors, the mechanical strength of the hydrogel electrolyte needs to be improved while maintaining a high level of stretchability and electrolyte adsorption ratio. Common poly(vinyl alcohol) (PVA) hydrogel electrolytes,[34−36] which are applied in flexible storage-energy devices, generally exhibit poor mechanical performance after adsorbing aqueous electrolyte. With anionic polyurethane acrylates as a multifunctional cross-linking agent, Na_2SO_4-anionic polyurethane acrylates/polyacrylamide (Na_2SO_4-*a*PUA/PAAM) hydrogel electrolyte exhibits improved mechanical strength of 74.5 kPa after adsorbing 500% aqueous electrolyte.[7] As another important method to enhance the mechanical properties of hydrogels, nanoparticles can be introduced either as a cross-linking agent or by being entrapped within the hydrogel network.[37−40]

Herein, vinyl group grafted-silica (CH_2═CH—SiO_2) nanoparticles were used as a nanoparticle cross-linker for polyacrylamide (PAAM), obtaining a nanocomposite hydrogel electrolyte of KCl—CH_2═CH—SiO_2/PAAM with a high strength of 844 kPa at the strain of 3400%. Besides, a high-performance carbon nanotube supported polypyrrole (CNT@PPy) film anode is prepared to match with the carbon nanotube supported manganese dioxide (CNT@MnO_2) film cathode. On the basis of the as-prepared highly conductive, sticky, and stretchable hydrogel electrolyte as well as the high-performance electrodes, we follow the "prestrain-stick-release"[7] assembly process to get the asymmetric stretchable CNT@MnO_2//KCl—CH_2═CH—SiO_2/PAAM//CNT@PPy supercapacitor. As a result, the potential window of the device is significantly enhanced to 0−2.0 V, and a high energy density of 40 Wh kg^{-1} is achieved at the power density of 519 kW kg^{-1} with the strain of 100%, which is the best known for the reported stretchable supercapacitors.

EXPERIMENTAL SECTION

Synthesis of Vinyl Group Grafted Silica (CH_2═CH—SiO_2) Nanoparticles. Vinyl group grafted silica is prepared following the one-pot procedure[41,42] shown in Supporting Information Figure S1. Tetraethoxysilane (TEOS, bought from Aladdin) and vinyltriethoxysilane (VTEOS, Aladdin) are used as precursor and coprecursor, respectively. Typically, 6 mL of $NH_3{\cdot}H_2O$ and 17.5 mL of H_2O were slowly added to 100 mL of C_2H_5OH at 40 °C to get homogeneous mixed solution A. Then, 6.4 mL of TEOS in 7.5 mL of C_2H_5OH (mixed solution B) was added suddenly to solution A under vigorous stirring. When the reaction mixture become turbid, VTEOS was added with different molar ratios of TEOS/VTEOS (95/5, 90/10, and 85/5), respectively, and then kept stirring for 30 min. Finally, the precipitates were washed with ethanol and dialyzed against deionized water for 5 days so as to obtain CH_2═CH—SiO_2 nanoparticles. Also, pure SiO_2 nanoparticles are prepared through a similar procedure without the addition of VTEOS.

It should be noted that if without specific description, the CH_2═CH—SiO_2 nanoparticles are prepared with the molar ratio of TEOS/VTEOS to be 90/10.

Preparation of KCl—CH_2═CH—SiO_2/PAAM Hydrogel Electrolyte. CH_2═CH—SiO_2/polyacrylamide (PAAM) hydrogel was prepared with the as-synthesized CH_2═CH—SiO_2 as a cross-linking agent for PAAM, and the scheme is shown in Supporting Information Figure S2. First, a certain amount of CH_2═CH—SiO_2 nanoparticles were ultrasonically dispersed in 12 mL of deionized water for 3 h, and then 2.0 g of acrylamide (AAM, Sigma-Aldrich) was added under ultrasonic dispersion for 2 h, during which argon gas was bubbled continuously so as to remove the air in the reaction system. Also, the amount of CH_2═CH—SiO_2 was adjusted to 4, 8, 12, 16, and 20 wt %, respectively. Second, 0.03 g of ammonium persulfate (APS, Aladdin) was added to the reaction system, and this was kept bubbling with argon gas to get rid of oxygen for 30 min. After that, the above mixed solution was injected to the mold of 100 × 100 × 1 mm^3 and evacuated to remove bubbles. Finally, the reaction was maintained under 70 °C for 3 h to form CH_2═CH—SiO_2/ PAAM hydrogel.

To get KCl—CH_2═CH—SiO_2/PAAM hydrogel electrolyte, the as-prepared CH_2═CH—SiO_2/PAAM hydrogel was immersed in deionized water for 24 h to remove redundant monomer of AAM or impurities, and then was dried under 50 °C. Finally, it was immersed in 1 M KCl for different times so as to obtain KCl—CH_2═CH—SiO_2/PAAM hydrogel electrolyte with various swelling ratios.

It should be noted that if without specific description, KCl—CH_2═CH—SiO_2/PAAM hydrogel electrolyte used in this paper is prepared under the optimal condition with 12 wt % CH_2═CH—SiO_2, and the swelling ratio is 600%. All the swelling ratios of the electrolyte mentioned in this paper are in the unit of mass.

Preparation of Carbon Nanotube Supported Polypyrrole (CNT@PPy) Anode and MnO_2 (CNT@MnO_2) Cathode. Both CNT@PPy and CNT@MnO_2 electrodes were prepared by electrodeposition method. Prior to electrodeposition, a CNT film (Suzhou Creative Nano-Carbon Co. Ltd.) was ultrasonically treated in ethanol and deionized water for 10 h so as to get a looser structure of the CNT film. Then, the as-treated CNT film of 25 × 10 mm^2, a platinum sheet of 20 × 20 mm^2, and saturated calomel electrode (SCE) were used as the working, counter, and reference electrodes, respectively.

For the CNT@PPy anode, the cathodic electrodeposition was carried out in a mixed solution of 0.02 M KCl, 0.001 M HCl, and 0.05 pyrrole at the constant potential of 0.7 V for 500, 1000, 1500, 2000, and 2500 s. It should be noticed that, prior to electrodeposition, the mixed solution was bubbled with argon gas so as to remove the oxygen. CNT@MnO_2 anode was prepared similarly in a mixed solution of 0.2 M KCl and 0.2 M $Mn(OOCCH_3)_2$ at the constant potential of 0.6 V, and the electrodeposition time was controlled to 400, 800, 1200, 1600 s.

It should be noted that if without specific description, the CNT@PPy and CNT@MnO_2 electrodes refer to those obtained at the electrodeposition time of 2000 and 1200 s, respectively.

Device Assembly of the Stretchable Supercapacitor. The assembly process of the stretchable supercapacitors followed the "prestrain-stick-release" strategy as reported in our previous paper,[7] and the process is also shown in Supporting Information Figure S3. The as-prepared KCl—CH_2═CH—SiO_2/PAAM hydrogel electrolyte with swelling ratio of 600% was prestretched to the tensile strain of 400%. Then, two CNT@PPy and CNT@MnO_2 films were adhered to two sides of the stretched hydrogel electrolyte closely. A sandwich-like CNT@MnO_2//KCl—CH_2═CH—SiO_2/PAAM//CNT@PPy stretchable supercapacitor was obtained by releasing the hydrogel electrolyte to get buckled films on its two sides. To test its electrochemical performance, two Pt sheets were covered closely on the film electrodes to function as current collectors.

Characterization. The morphologies of the samples were observed by field-emission scanning electron microscope (FE-SEM, Hitachi S-4800). The Fourier transform infrared spectroscopy (FT-IR)

DOI: 10.1021/acsami.5b03148
ACS Appl. Mater. Interfaces 2015, 7, 15303−15313

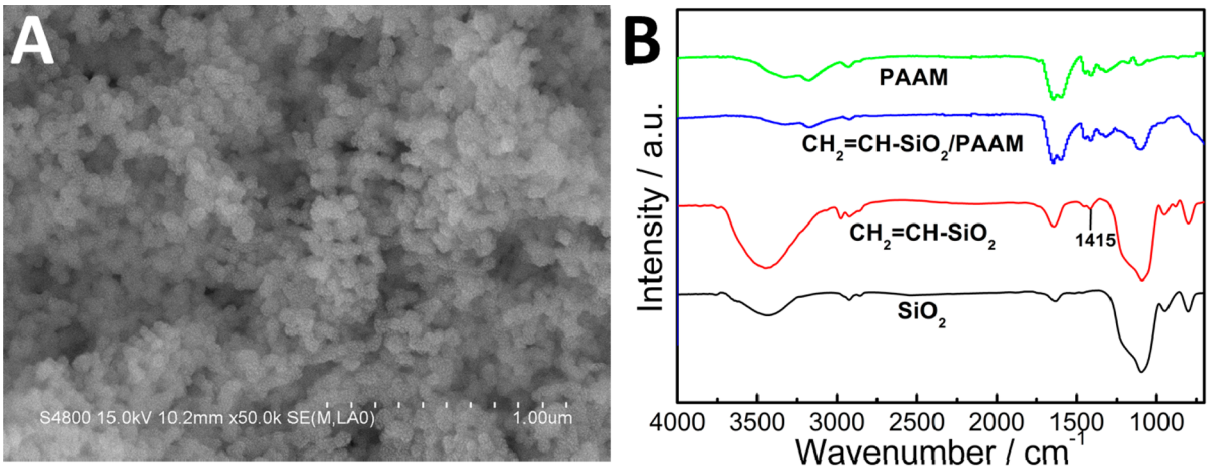

Figure 1. (A) FE-SEM images of CH_2═CH—SiO_2 and (B) FT-IR spectra of SiO_2, CH_2═CH—SiO_2, CH_2═CH—SiO_2/PAAM hydrogel and PAAM hydrogel after drying.

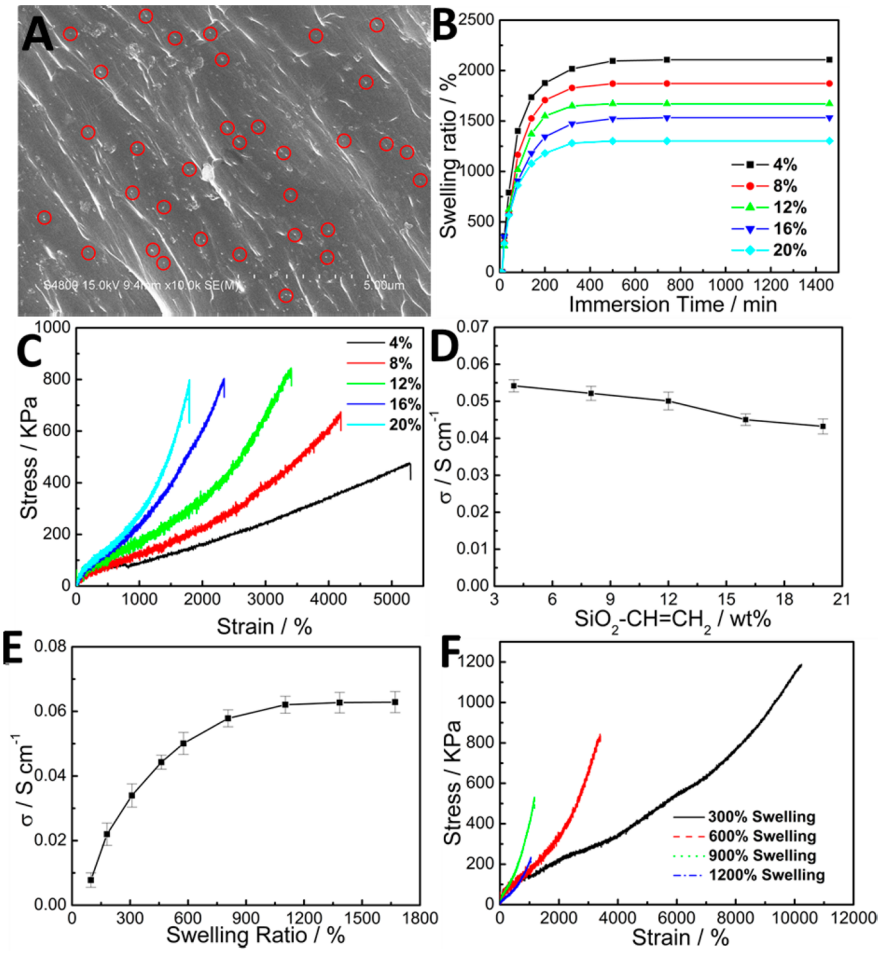

Figure 2. (A) FE-SEM images of CH_2═CH—SiO_2/PAAM hydrogel, (B) swelling ratio of KCl—CH_2═CH—SiO_2/PAAM hydrogel electrolyte versus various immersion time with different CH_2═CH—SiO_2 weight ratio, (C) stress−strain curves, and (D) ionic conductivity of KCl—CH_2═CH—SiO_2/PAAM hydrogel electrolyte with different CH_2═CH—SiO_2 weight ratio at the swelling ratio of 600%, (E) ionic conductivity, and (F) stress−strain curves for KCl—CH_2═CH—SiO_2/PAAM hydrogel electrolyte with 12% CH_2═CH—SiO_2 under different swelling ratios.

spectra were collected using a Nicolet 6700 spectrometer equipped with a Smart OMNI sampler. Powder X-ray diffraction (XRD) patterns were performed in a Rigaku D/Max 2550 VB/PC X-ray diffractometer using Cu ($K\alpha$) radiation. The mechanical properties of the KCl—CH_2═CH—SiO_2/PAAM hydrogel electrolytes was measured on a Zwick Roell testing system at a stretching speed of 100 mm min^{-1}. Digital photos were taken by Nikon COOLPIX S6300. The ionic conductivity of the hydrogel electrolyte is obtained by the equation of $\sigma = I/R_bA$, where I is the thickness (cm) of the hydrogel, A is the contact area (cm^2) of the hydrogel electrolyte with the current collectors, and R_b is the bulk resistance (Ω) obtained from the first intercept on the x-axis of the impedance figures (shown in Supporting

DOI: 10.1021/acsami.5b03148
ACS Appl. Mater. Interfaces 2015, 7, 15303−15313

Information Figure S4). Also, the bulk resistance (Ω) of R_b is measured by sandwiching the hydrogel with two Pt sheets of 10 × 20 mm^2 as current collectors on a CHI 660D electrochemical workstation.

Electrochemical Measurements. Cyclic voltammetry (CV), galvanostatic charge−discharge, and electrochemical impedance spectroscopy (EIS) measurements were performed on a CHI 660D electrochemical workstation. Also, the cycling stability was measured on a program testing system (LAND CT2001A).

For the three-electrode mode measurement, the prepared film electrode was used directly as working electrode with a saturated calomel electrode (SCE) reference electrode and a Pt counter electrode. The electrolyte was 1 M KCl aqueous solution. The specific areal capacitance of the film electrode is calculated by the three-electrode data following

$$C_s = C/A = I\Delta t/A\Delta V$$

where I is the discharge current, A is the area of the film electrode, Δt is the discharging time, and ΔV is the voltage change during the discharging time after IR drop. The two-electrode mode measurement was carried out to get the electrochemical performance of the fully stretchable supercapacitor device. Also, the specific areal capacitance of the full supercapacitor device is calculated on the basis of the two-electrode mode data following the equation below as well. For the specific mass capacitance (C_T) of the supercapacitor device, it can be calculated from charge/discharge curve according to

$$C_T = I\Delta t/(m\Delta V)$$

where I is the discharge current, Δt is the discharge time, and ΔV is the voltage change upon discharge (excluding IR drop), and m is the total mass of electroactive material (the supported MnO_2 and PPy components) of two electrodes. The energy density (E) and power density (P) for a supercapacitor cell can be estimated using the following the equations of $E = {}^1/_2 C_T \Delta V^2$ and $P = E/\Delta t$, respectively.

RESULTS AND DISCUSSION

PAAM hydrogel is often used in solid electrolyte for supercapacitors. However, the weak mechanical strength of non-cross-linking PAAM after adsorbing enough aqueous electrolyte restricts its application in stretchable supercapacitors.[43] Herein, vinyl group grafted silica (CH_2═CH—SiO_2) is introduced as a nanoparticle cross-linker to strengthen PAAM hydrogel. As shown in Figure 1A, CH_2═CH—SiO_2 nanoparticles exhibit a homogeneous diameter of about 70 nm, while nonmodified SiO_2 nanoparticles (Supporting Information Figure S5) show more random size distribution with both large and small ones. The smaller and more homogeneous diameter of CH_2═CH—SiO_2 nanoparticles is due to the fact that VTEOS is more prone to anchor onto the cores of primary silica particles compared with TEOS, forming a vinyl organic shell on the surface of silica cores and inhibiting the regrowing of these particles and the Ostwald ripening process.[41] From the corresponding FT-IR spectra (Figure 1B), we can see that both SiO_2 and CH_2═CH—SiO_2 nanoparticles exhibit main characteristic peaks at about 1100, 950, and 795 cm^{-1}, which are assigned to $\nu_{(Si-O-Si)}$, $\nu_{(Si-OH)}$, and $\delta_{(Si-O-Si)}$, respectively.[39] The peak at 3425 cm^{-1} is ascribed to the $\nu_{(O-H)}$ of silica nanoparticles and H_2O. For CH_2═CH—SiO_2 nanoparticles, the additional peaks at 1415 cm^{-1} correspond well to assignment of the bending deformation of CH_2═CH groups, confirming the successful grafting of vinyl group to silica nanoparticles.[41] For PAAM and CH_2═CH—SiO_2/PAAM hydrogel, the bands at 1653 and 1606 cm^{-1} are attributed to the amide I vibration (δ_{N-H}) and amide II vibration ($\upsilon_{C=O}$) of PAAM, respectively.[44] We also studied the effect of the TEOS/VTEOS molar ratio on the morphology of the CH_2═CH—SiO_2 as well as the mechanical performance of the KCl—CH═CH_2—SiO_2/PAAM hydrogel electrolytes (Supporting Information Figure S6). With the TEOS/VTEOS molar ratio from 95/5, 90/10, to 85/15, the elongation at break decreases, while the tensile strength of the CH═CH_2−SiO_2/PAAM hydrogel first increases and then almost remains unchanged. Thus, the TEOS/VTEOS molar ratio of 90/10 was chosen for further study due to the optimal mechanical performance of the corresponding KCl—CH═CH_2−SiO_2/PAAM hydrogel electrolytes.

From Figure 2A, it is obvious that CH_2═CH—SiO_2 nanoparticles (with the red circles pointed) are homogeneously distributed in CH_2═CH—SiO_2/PAAM hydrogel. From its synthesis scheme shown in Supporting Information Figure S2, end-vinyl groups of CH_2═CH—SiO_2 nanoparticles function as cross-linking points for PAAM. To confirm the successful chemical cross-linking of CH_2═CH—=SiO_2/PAAM hydrogel, we also immersed it in deionized water at 50 °C for 12 h. It is found that the CH_2═CH—SiO_2/PAAM hydrogel shows only swelling (Supporting Information Figure S7A), while pure PAAM hydrogel is severely damaged with most of its component dissolving (Supporting Information Figure S7B). The above results confirm the chemical cross-linking in the CH_2═CH-SiO_2/PAAM hydrogel. Besides, we compared the mechanical performance of KCl—CH═CH_2−SiO_2/PAAM hydrogel with KCl—SiO_2/PAAM hydrogel. We can see from Supporting Information Figure S8 that the tensile strength of the KCl—CH═CH_2−SiO_2/PAAM hydrogel increases to 843 kPa compared with 400 kPa of SiO_2/PAAM hydrogel. Apart from physcial cross-linking, the SiO_2−CH═CH_2 nanoparticles also function as chemical cross-linking points, leading to the increase of tensile strength. Besides, larger chemical cross-linking density restricts the movement of the polymer chain, and the elongation at the break of KCl—CH═CH_2−SiO_2/PAAM hydrogel shows a little decrease to 3400% compared with KCl—SiO_2/PAAM hydrogel of 4720%.

Furthermore, it is found that, with the amount of CH_2═CH—SiO_2 increasing from 4 to 20 wt %, KCl—CH_2═CH-SiO_2/PAAM hydrogel electrolyte shows smaller swelling ratio equilibrium (shown in Figure 2B), which is due to its higher cross-linking density. Furthermore, in Figure 2C,D, it can be seen that, with more CH_2═CH—SiO_2 nanoparticles added, the elongation at the break of the as-prepared hydrogel electrolytes gradually decreases from 5300% to 1800%, and the electronic conductivity slightly decreases from 0.054 to 0.043 S cm^{-1} while for the tensile strength, it first increases with the CH_2═CH—SiO_2 nanoparticle content increasing from 4% to 12 wt %, and thereafter, it gradually decreases. On the basis of the above results, 12 wt % CH_2═CH—SiO_2 content is chosen with a balance between mechanical and electrical properties. Herein, with more CH_2═CH—SiO_2 nanoparticles added from 4 to 12 wt %, the cross-linking density of the obtained hydrogel electrolyte increases, leading to enhanced tensile strength. However, with a further increase in the amount of CH_2═CH—SiO_2 nanoparticles from 12 to 20 wt %, the cross-linking density approaches saturation and CH_2═CH—SiO_2 nanoparticles tend to agglomerate which leads to the defect of the hydrogel electrolyte, leading to a decrease of tensile strength. Also, the decrease of the elongation at break is mainly attributed to the larger chemical and physical cross-linking density restricting the movement of polymer chains.

We also conducted experiments to determine the optimal swelling ratio for the as-prepared hydrogel electrolyte. Figure

DOI: 10.1021/acsami.5b03148
ACS Appl. Mater. Interfaces 2015, 7, 15303−15313

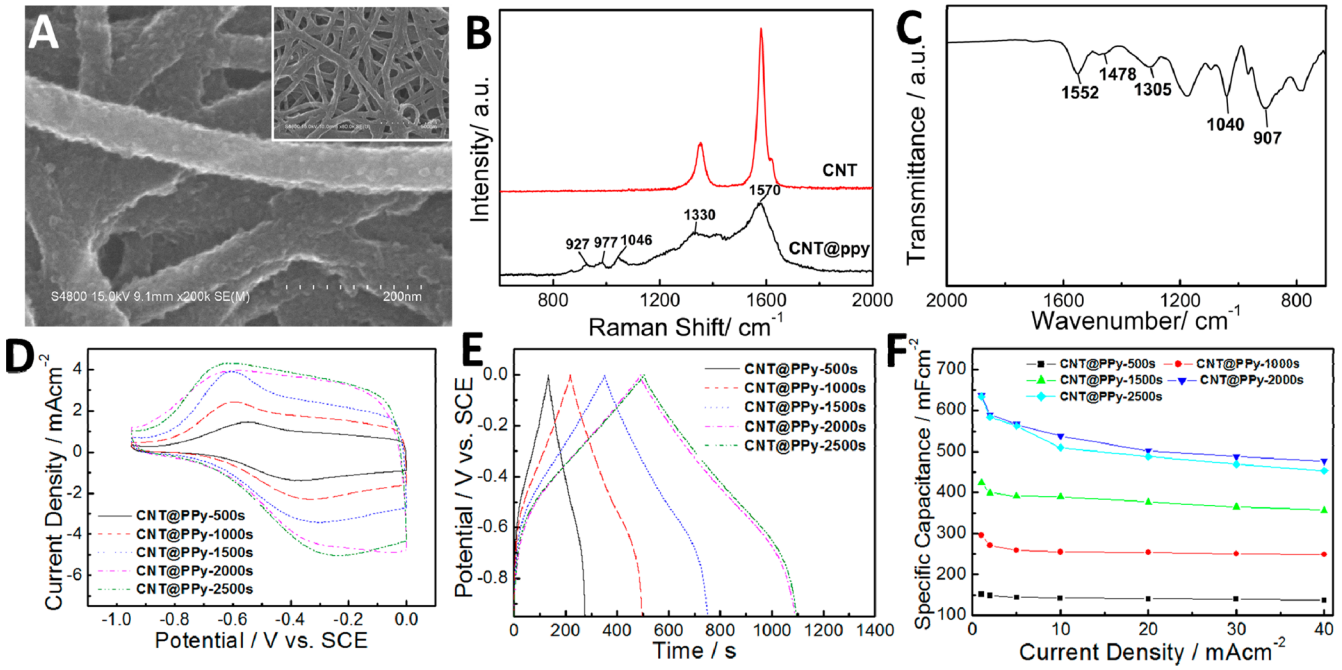

Figure 3. (A) FE-SEM image of the CNT@PPy film electrode (inserted with the corresponding FE-SEM image of smaller magnification), (B) Raman spectrum of CNT film and CNT@PPy film, (C) ATR-FTIR spectra of CNT@PPy film, the electrochemical performance of the CNT@PPy film electrode with various electrodeposition times, (D) CV curves at a scan rate of 5 mV s^{-1}, (E) GCD curves at a current density of 1 mA cm^{-2}, and (F) specific capacitance at various current densities from 1 to 40 mA cm^{-2}.

2E shows that the electronic conductivity of the KCl—CH_2=CH—SiO_2/PAAM hydrogel electrolyte significantly improved from 7.82×10^{-3} to 0.050 S cm^{-1} with swelling ratio from 97% to 576%, and further immersing it in aqueous electrolyte shows no obvious enhancement for conductivity. While for mechanical performance, it sharply decreases with larger swelling ratio as shown in Figure 2F. Thus, 600% swelling ratio is viewed as the most suitable for practical usage for stretchable hydrogel electrolyte. To investigate the long-term stretchability of the hydrogel electrolyte, we also conducted cycles of elongation−relaxation experiments on the KCl—CH_2=CH—SiO_2/PAAM hydrogel electrolyte. As shown in Supporting Information Figure S9, the plastic deformation is only 10.1% after 2000 cycles, and the conductivity changes slowly, indicating its excellent stability in the plastic deformation and conductivity. Also, the slow decrease of the performance is mainly due to the evaporation of water of the hydrogel electrolyte with the self-constructed device.

From the above discussion, we can find that introduction of CH_2=CH—SiO_2 significantly improves the mechanical performance of PAAM. Even in a comparison with highly stretchable Na_2SO_4-*a*PUA/PAAM[7] (tensile strength of 74.5 kPa, elongation at break of 970%), the KCl—CH_2=CH—SiO_2/PAAM hydrogel electrolyte shows more excellent mechanical strength with a high tensile strength of 843 kPa and an elongation at break of 3400%, confirming that CH_2=CH—SiO_2 nanoparticles are more effective cross-linking agents to improve the mechanical performance. Both physical cross-linking with hydrogel bonding and chemical cross-linking between CH_2=CH—SiO_2 nanoparticles and PAAM contributed to this significant strength enhancement.[40,45,46] To function as the hydrogel electrolyte, the strong stickiness of the KCl—CH_2=CH—SiO_2/PAAM hydrogel electrolyte should also be ensured so as to have close interface contact with film electrodes. As shown in Supporting Information Figure S10, after the hydrogel electrolyte was stretched to 200%, the film electrode is still strongly adhered to it without separation. Besides, after the hydrogel was stretched to break, the breaking points lie in the hydrogel rather than at the interface with the films, confirming the strong stickiness of KCl—CH_2=CH—SiO_2/PAAM hydrogel electrolyte to the films. And the origin of the strong stickiness has been explained with details in our previous paper.[7]

In order to enhance the energy density of the stretchable supercapacitor, we aimed to assemble an asymmetric device with broadening potential window. PPy exhibits good electrochemical performance in the negative potential range, making it a good candidate for the anodes of supercapacitors. Herein, PPy is electrodeposited onto CNT film to obtain the CNT@PPy anode. Supporting Information Figure S11 shows the pure CNT film with a smooth surface, while the CNT@PPy film (Figure 3A) exhibits a rough surface with PPy particles on the CNT. The inserted image also shows the network structure of the as-prepared film, which is beneficial for electrolyte penetration to the surface of electrode. Besides, Raman and ATR-FTIR spectra were utilized to study the structure of the CNT@PPy film. In Raman spectrum (Figure 3B), CNT displays two prominent bands at 1585 and 1355 cm^{-1}, corresponding to the G and D bands, respectively. For the CNT@PPy film, the peaks at 1570 and 1330 cm^{-1} arise from the π conjugated structure and ring stretching mode of the PPy backbone, respectively. The broad peak near 1046, 927, and 977 cm^{-1} corresponds to the C—H in-plane deformation, and the quinoid polaronic and bipolaronic structure of the deposited PPy, respectively.[47] The weakening of the CNT-related peaks can be ascribed to the fact that PPy is deposited on the surface of CNT. The ATR-FTIR spectrum (Figure 3C) of the CNT@PPy film exhibits characteristic peaks at 1552, 1478, 1305, 1040, 907 cm^{-1}, which are assigned to C=C stretching, C—N stretching, C—N in-plane deformation, and

DOI: 10.1021/acsami.5b03148
ACS Appl. Mater. Interfaces 2015, 7, 15303−15313

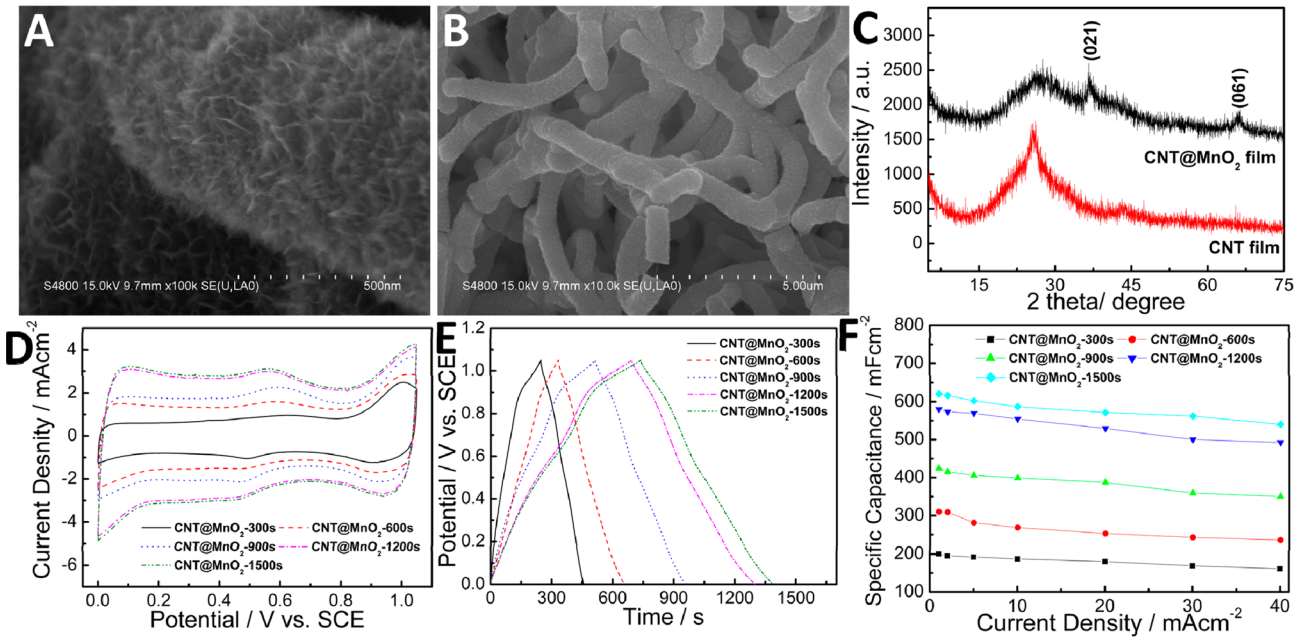

Figure 4. (A, B) FE-SEM images of the CNT@MnO_2 film with large and small magnification, (C) XRD pattern of the CNT and CNT@MnO_2 film, the electrochemical performance of the CNT@MnO_2 film electrode with various electrodeposition times, (D) CV curves at a scan rate of 5 mV s^{-1}, (E) GCD curves at a current density of 1 mA cm^{-2}, and (F) specific capacitance at various current densities from 1 to 40 mA cm^{-2}.

C—H in-plane and out-of-plane deformation vibration in the pyrrole ring,[48,49] respectively. The above results indicate that the PPy species are successfully deposited onto the surface of CNTs.

The electrochemical performance of the as-synthesized CNT@PPy films as the electrodes are investigated by cycle voltammetry (CV) and galvanostatic charge−discharge (GCD) tests. It is found that, with increasing electropolymerization time from 500 to 2000 s, the CV curves (Figure 3D,E) show larger integral area, and the GCD curves shows longer discharge time in the negative potential window of 0 to −0.95 V, which indicates the enhancement of the specific capacitance with more deposited PPy. When further improving the electropolymerization time to 2500 s, the CV and GCD curves almost coincide with the ones for 2000 s, showing no further increase of specific capacitance. This phenomenon may be due to the deposited PPy tending to aggregate with longer deposition time, decreasing the utilization rate of the electrochemical active component. On the basis of the GCD tests, the corresponding calculated specific capacitance is provided in Figure 3F. At the electrodeposition time of 2000 s, the CNT@PPy film shows a large specific areal capacitance of 637 mF cm^{-2} at the current density of 1 mA cm^{-1} and good rate performance with capacitance retention rate of 75% up to 40 mA cm^{-1}. Thus, the electrodeposition time of 2000 s is chosen as optimal for the CNT@PPy film.

To match the CNT@PPy anode, the CNT@MnO_2 film as cathode is prepared with the similar electrodeposition process. From Figure 4A,B, it is quite obvious that loosely packed MnO_2 nanoflakes are grown on the surface of the CNT, significantly increasing the diameter to about 500 nm compared with the pure CNT of 10−50 nm. The XRD pattern (Figure 4C) of the CNT@MnO_2 film exhibits two additional peaks corresponding to (021) and (061) crystal planes of γ-MnO_2[50] apart from the broad amorphous holo of CNT at 15−40°.

From the CV curves (Figure 4D), the CNT@MnO_2 film shows weak redox peaks in the positive potential window of 0−1.05 V, which is related to the valent state change during charging and discharging. Also, the corresponding GCD (Figure 4E) curves also exhibit a slight charging−discharging plateau. Furthermore, for the assembly of the asymmetric supercapacitor, it should follow the charge balance relationship of $q^+ = q-$ between cathodes and anodes. The charge can be expressed according to $q = C_s \times \Delta V \times A$, where C_s is the specific areal capacitance, ΔV is the potential window, and A is the area of the electrode. Since the CNT@PPy anode and the CNT@MnO_2 cathode exhibit the same film area, we should make sure that they satisfy the equation "$C_s^+ \times \Delta V^+ = C_s \times \Delta V^-$". Thus, the specific areal capacitance of the CNT@MnO_2 cathode should be around 576 mF cm^{-2} at the current density of 1 mA cm^{-2} ($C_s^+ = C_s^- \times \Delta V^-/\Delta V^+$). From Figure 4F, we can see that the electrodeposition time of 1200 s is suitable for the CNT@MnO_2 cathode with appropriate specific capacitance of 580 mF cm^{-2} at 1 mA cm^{-2}.

On the basis of the as-prepared KCl—CH_2═CH—SiO_2/PAAM hydrogel electrolyte with excellent mechanical performance and the CNT@PPy anode and the CNT@MnO_2 cathode with matching potential window, we followed the "prestrain-stick-release" strategy[7] to assemble the stretchable asymmetric supercapacitor. As shown in Supporting Information Figure S3, the assembled CNT@MnO_2//KCl—CH_2═CH—SiO_2/PAAM//CNT@PPy stretchable supercapacitor exhibits a sanwiched structure with two buckled film electrodes closely adhered to the sticky hydrogel electrolyte (Figure 5A). Besides, taking advantage of the excellent stretchability of the hydrogel electrolyte and the resilient property of the CNT-based film electrodes, the as-assembled stretchable asymmetric supercapacitor can be easily stretched to 100% strain (Figure 5B) or twisted to a large angle of 90° (Figure 5C).

To investigate the electrochemical performance of the CNT@MnO_2//KCl—CH_2═CH—SiO_2/PAAM//CNT@PPy stretchable asymmetric supercapacitor, the measurements for CV and GCD curves were conducted within different potential windows with the strain of 100%. With increasing potential

DOI: 10.1021/acsami.5b03148
ACS Appl. Mater. Interfaces 2015, 7, 15303−15313

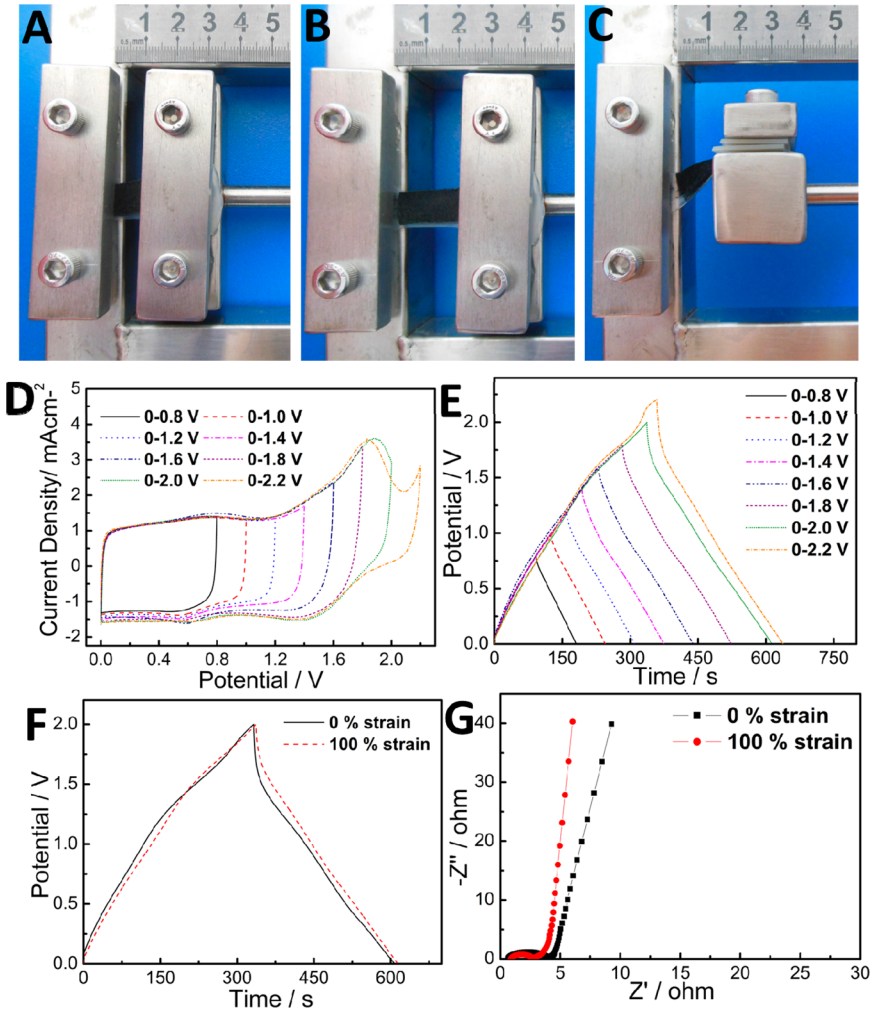

Figure 5. Digital photos showing different states of the CNT@MnO_2//KCl—CH_2═CH—SiO_2/PAAM//CNT@PPy stretchable asymmetric supercapacitor: (A) initial state, (B) stretchable state at the 100% strain, and (C) twisted state at 90°. Electrochemical performance of the CNT@MnO_2//KCl—CH_2═CH—SiO_2/PAAM//CNT@PPy stretchable asymmetric supercapacitor at the strain of 100%: (D) CV at a scan rate of 5 mVs^{-1} and (E) GCD curves at a current density of 1 mA cm^{-2} within different potential windows, and (F) GCD curves at 1 mA cm^{-2} and (G) Nyquist plots in frequency ranging from 100 kHz to 0.1 Hz at 0 and 100% strains.

limit from 0.8 to 2.0 V, CV curves (Figure 5D) exhibit more obvious redox peaks and larger integral area, indicating more pseudocapacitance. However, when the potential limit was further improved to 2.2 V, the CV curves become distorted at the high potential arising from decomposition of water. The GCD curves (Figure 5E) exhibit a symmetric charging and discharging plot up to the potential of 2.0 V indicating the good reversible properties of the electrochemical process. Besides, it exhibits a negligible IR drop of 0.029 V (the enlarged figure provided in Supporting Information Figure S12), while GCD curves tend to flatten approaching 2.2 V, which is ascribed to the irreversible electrochemical reaction and is in accordance with the CV curves. Thus, 0−2.0 V is chosen as the safe potential window for the assembled stretchable asymmetric supercapacitor.

To study the influence of stretching, we compared the electrochemical performance of the as-fabricated supercapacitor at 0 and 100% strains. As shown in Figure 5 F, the GCD curves at 0 and 100% strains are quite close to each other with almost the same charging−discharging time. For the Nyquist plots (Figure 5G), the supercapacitors at 0 and 100% strains exhibit small semicircle diameter followed by nearly vertical lines, indicating low charge transfer resistance due to the strong stickiness of the hydrogel electrolyte to the film electrodes as well as the relative ideal capacitive behavior. Besides, it is interesting to find that the supercapacitor at 100% strain exhibits a slightly smaller contact resistance of 0.8 Ω (the intercept at the real axis), and a lower charge transfer resistance of 1.9 Ω (the semicircle diameter) as well as a more vertical line in the low frequencies. This phenomenon is in analogy with our previous reports for stretchable supercapacitors,[7] and it may be due to the film electrodes being more closely attached to the hydrogel electrolyte under strains.

We also measured the electrochemical performance of the CNT@MnO_2//CNT@PPy stretchable supercapacitors after various stretching−relaxation cycles. As can be seen from Supporting Information Figure S13A, with more stretching−relaxation cycles, the Nyquist plots exhibit a semicircle with slowly increasing diameter, showing an increasing charge transfer resistance of the stretchable supercapacitor. This phenomenon is mainly due to the fact that the film electrodes are more loosely attached to the hydrogel electrolyte. Even so, we can still see from the Nyquist plot that, after 500 stretching−relaxation cycles, the CNT@MnO_2//CNT@PPy

DOI: 10.1021/acsami.5b03148
ACS Appl. Mater. Interfaces 2015, 7, 15303−15313

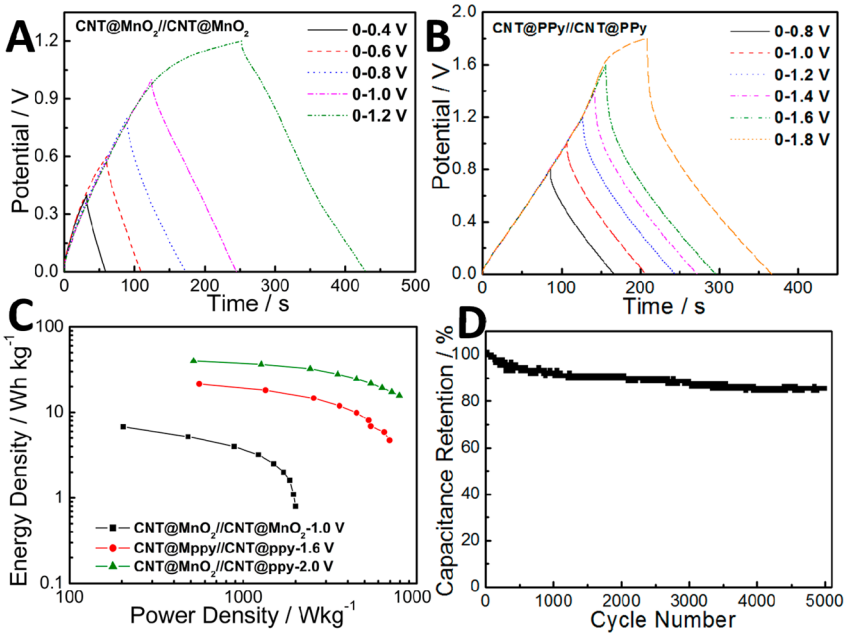

Figure 6. GCD curves within different potential windows at the 100% strain for the (A) CNT@MnO_2//CNT@MnO_2 and (B) CNT@PPy//CNT@PPy stretchable supercapacitors. (C) Ragone plots at the 100% strain for the CNT@MnO_2//CNT@MnO_2, CNT@PPy//CNT@PPy, and CNT@MnO_2//CNT@PPy stretchable supercapacitors, and (D) cycling stability at a current density of 4 mA cm^{-2} for the CNT@MnO_2//CNT@PPy stretchable asymmetric supercapacitor at the 100% strain.

stretchable supercapacitor exhibits a small contact resistance of 0.7 Ω (the intercept at the real axis), and a low charge transfer resistance of 3.2 Ω (the semicircle diameter) as well as a vertical line in the low frequencies, confirming the good supercapacitive retention behavior. Besides, it still retains a specific capacitance of 270 F g^{-1} after 500 stretching−relaxation cycles (calculated from Supporting Information Figure S13B), which is 96% of the initial state, confirming the excellent stretching−relaxation cycling stability. This is mainly due to good stretching−relaxation stability of the KCl—CH_2═CH—SiO_2/PAAM hydrogel electrolyte as well as its strong stickiness to the film electrodes.

To confirm the advantages of the asymmetric assembly of the CNT@MnO_2//KCl—CH_2═CH—SiO_2/PAAM//CNT@PPy stretchable supercapacitor, we compared its electrochemical performance with its corresponding symmetric devices of CNT@MnO_2//KCl—CH_2═CH-SiO_2/PAAM//CNT@MnO_2 and CNT@PPy//KCl—CH_2═CH—SiO_2/PAAM//CNT@PPy. In short, we neglected "KCl—CH_2═CH—SiO_2/PAAM" in their titles for these three stretchable supercapacitors in the next discussion for Figure 6 and Supporting Information Figure S14. First, to determine the appropriate potential windows for CNT@MnO_2//CNT@MnO_2 and CNT@PPy//CNT@PPy stretchable supercapacitors with the strain of 100%, GCD curves within different potential windows are shown in Figure 6A,B. It can be seen clearly that their charging curves tend to flatten approaching the potential limit of 1.2 and 1.8 V, respectively, indicating the irreversible electrochemical reaction at these potentials. Thus, 0−1.0 and 0−1.6 V are chosen for CNT@MnO_2//CNT@MnO_2 and CNT@PPy//CNT@PPy stretchable supercapacitors, respectively.

Besides, GCD curves for the assembled stretchable supercapacitors of CNT@MnO_2//CNT@MnO_2 in 0−1.0 V, CNT@PPy//CNT@PPy in 0−1.6 V, and CNT@MnO_2//CNT@PPy in 0−2.0 V at different current densities from 2 to 40 mA cm^{-2} with the strain of 100% are provided in Supporting Information Figure S14A−C. Also, the specific capacitances (Supporting Information Figure S14D) for the three stretchable supercapacitors are calculated on the basis of the GCD curves. The CNT@MnO_2//CNT@PPy stretchable supercapacitor exhibits a specific capacitance of 281.3 mF cm^{-2} at 2 mA cm^{-2} and a high capacitance retention rate of 67.3% up to 40 mA cm^{-2}. Furthermore, the energy and power density performance is the major evaluation criteria for the practical application of energy storage devices. On the basis of the fact that the specific areal masses of electroactive component for the CNT@MnO_2 cathode and CNT@PPy anode are 2.4 and 1.4 mg cm^{-2}, respectively, the Ragone plots (energy density vs power density) are given in Figure 6C. It is quite obvious that the CNT@MnO_2//CNT@PPy stretchable asymmetric supercapacitor exhibits much higher energy density than the corresponding two symmetric devices, achieving 40.0 Wh kg^{-1} at 519 kW kg^{-1} and still retaining 15.8 Wh kg^{-1} at 8000 kW kg^{-1}, while for CNT@MnO_2//CNT@MnO_2 and CNT@PPy//CNT@PPy, they display 21.5 Wh kg^{-1} at 558 kW kg^{-1} and 6.8 Wh kg^{-1} at 204 kW kg^{-1}, respectively. Thus, it can be concluded that the asymmetric assembly based on the perfect matching of CNT@MnO_2 and CNT@PPy can significantly enhance the energy density of the device. This improvement is mainly due to the broadening of the potential window to 2.0 V and the full utilization of the capacitance of both the cathodes and anodes.

In addition, we compared the electrochemical performance of the CNT@MnO_2//CNT@PPy stretchable asymmetric supercapacitor with previously reported stretchable supercapacitors. The highest energy density having been reported for stretchable supercapacitor is 15.7 Wh kg^{-1} with the use of an ionic-liquid-based nonvolatile gel (ion-gel) electrolyte with a broad potential window of 0−3.0 V.[9] The symmetric pseudocapacitors with polyaniline-based electrodes and H_2SO_4/PVA hydrogel electrolyte display 9 and 11 Wh

DOI: 10.1021/acsami.5b03148
ACS Appl. Mater. Interfaces 2015, 7, 15303−15313

kg^{-1}.[51,52] Other reported stretchable ones exhibit much smaller energy densities mainly in the range 0.9−4.5 Wh kg^{-1}.[7,26,53] Thus, it is quite obvious that the as-assembled CNT@MnO_2//CNT@PPy stretchable asymmetric supercapacitor displays the most excellent energy performance ever reported.

As for practical application, specific volumetric capacitance and energy density are also of great significance. The assembled stretchable supercapacitor is about 1.5 mm. On the basis of the above data, we also calculated the specific volumetric capacitance and energy density of the CNT@MnO_2//CNT@PPy stretchable supercapacitor as shown in Supporting Information Figure S15. It exhibits a specific volumetric capacitance of 2.2 F cm^{-3} at 2 mA cm^{-2}. Besides, it obtains a high energy density of 0.31 mWh cm^{-3} at the power density of 4.0 mWh cm^{-3}. The obtained electrochemical performance of the CNT@MnO_2//CNT@PPy stretchable supercapacitor is relatively excellent compared with those of previously reported stretchable ones. For example, the PANI-based stretchable device exhibits specific volumetric capacitance of about 1.4 F cm^{-3} and an energy density of 0.15 mWh cm^{-3} at 2 mA cm^{-2},[52] and the MnO_2/carbon particles-based one shows an energy density of 0.09 mWh cm^{-3}.[54]

Finally, we measured the capacitance retention rate of the CNT@MnO_2//CNT@PPy supercapacitor within 5000 cycles as cycling stability is the key property for the practical application of supercapacitors. As can been seen from Figure 6D, it shows an initial capacitance decrease of 9% in the first 1000 charging−discharging cycles. After that, the capacitance tends to stabilize, and the whole supercapacitor retains 85% of its capacitance after 5000 cycles, confirming its excellent cycling stability.

CONCLUSION

In summary, we have prepared a nanocomposite hydrogel electrolyte of KCl—CH_2=CH—SiO_2/PAAM with the end-vinyl group grafted-silica (CH_2=CH—SiO_2) nanoparticles as a nanoparticle cross-linker for the polymerization of acrylamide, significantly enhancing the tensile strength of PAAM to 844 kPa at the strain of 3400%, which is the most excellent reported for hydrogel electrolytes. Besides, taking advantage of the excellent stickiness and stretchability of the prepared hydrogel electrolytes, we matched the CNT@MnO_2 film cathode with the CNT@PPy film anode which shares compatible potential windows, and followed the "prestrain-stick-release" strategy[7] to assemble the CNT@MnO_2//KCl—CH_2=CH—SiO_2/PAAM//CNT@PPy stretchable asymmetric supercapacitor. As a result, the asymmetric device displays remarkably enhanced energy density of 40.0 Wh kg^{-1} within the broad potential window of 2.0 V at 100% strain, which is several factors or even orders higher than previous reported stretchable supercapacitors. The whole supercapacitor cell also exhibits good cycling stability of 85% capacitance retention rate after 5000 charging−discharging cycles. Thus, it can be anticipated that the excellent mechanical and electrochemical performance of the as-assembled stretchable asymmetric supercapacitor may provide a hint for the practical application of highly stretchable devices.

ASSOCIATED CONTENT

Supporting Information

Synthesis procedure for the vinyl grafted silica nanoparticles. Synthesis scheme for the CH_2=CH—SiO_2/polyacrylamide (PAAM) hydrogel. Digital photos showing the "prestrain-stick-release" process for the assembly of the CNT@MnO_2//KCl—CH_2=CH—SiO_2/PAAM//CNT@PPy stretchable supercapacitor. Nyquist plots of KCl—CH_2=CH—SiO_2/PAAM hydrogel electrolyte with different CH_2=CH—SiO_2 weight ratio at the swelling ratio of 600% and with different swelling ratio. Digital photos of CH_2=CH—SiO_2/PAAM and PAAM hydrogel after immersion in deionized water at 50 °C for 12 h. FE-SEM image of nonmodified SiO_2 nanoparticles. FE-SEM image of pure carbon nanotube (CNT) film. Electrochemical performance of the assembled CNT@MnO_2//CNT@MnO_2, CNT@PPy//CNT@PPy, and CNT@MnO_2//CNT@PPy stretchable supercapacitors at different current densities from 2 to 40 mA cm^{-2}. The Supporting Information is available free of charge on the ACS Publications website at DOI: 10.1021/acsami.5b03148.

AUTHOR INFORMATION

Corresponding Author

*Phone: +86-21-64253527. E-mail: gengchaow@ecust.edu.cn.

Notes

The authors declare no competing financial interest.

ACKNOWLEDGMENTS

We greatly appreciate the financial support of the National Natural Science Foundation of China (51173042), and Shanghai Municipal Science and Technology Commission (12 nm0504102).

REFERENCES

(1) Wu, Q.; Xu, Y.; Yao, Z.; Liu, A.; Shi, G. Supercapacitors Based on Flexible Graphene/Polyaniline Nanofiber Composite Films. *ACS Nano* **2010**, *4*, 1963−1970.

(2) Liu, S.; Wang, Z.; Yu, C.; Wu, H. B.; Wang, G.; Dong, Q.; Qiu, J.; Eychmueller, A.; Lou, X. W. A Flexible TiO_2(B)-Based Battery Electrode with Superior Power Rate and Ultralong Cycle Life. *Adv. Mater.* **2013**, *25*, 3462−3467.

(3) Lee, S. Y.; Choi, K. H.; Choi, W. S.; Kwon, Y. H.; Jung, H. R.; Shin, H. C.; Kim, J. Y. Progress in Fexible Energy Storage and Conversion Systems, with a Focus on Cable-type Lithium-ion Batteries. *Energy Environ. Sci.* **2013**, *6*, 2414−2423.

(4) He, Y.; Chen, W.; Li, X.; Zhang, Z.; Fu, J.; Zhao, C.; Xie, E. Freestanding Three-Dimensional Graphene/MnO_2 Composite Networks As Ultra light and Flexible Supercapacitor Electrodes. *ACS Nano* **2013**, *7*, 174−182.

(5) Lu, X.; Yu, M.; Wang, G.; Tong, Y.; Li, Y. Flexible Solid-state Supercapacitors: Design, Fabrication and Applications. *Energy Environ. Sci.* **2014**, *7*, 2160−2181.

(6) Xie, K.; Wei, B. Materials and Structures for Stretchable Energy Storage and Conversion Devices. *Adv. Mater.* **2014**, *26*, 3592−3617.

(7) Tang, Q. Q.; Chen, M. M.; Wang, G. C.; Bao, H.; Saha, P. A Facile Prestrain-stick-release Assembly of Stretchable Supercapacitors Based on Highly Stretchable and Sticky Hydrogel Electrolyte. *J. Power Sources* **2015**, *284*, 400−408.

(8) Chen, T.; Hao, R.; Peng, H. S.; Dai, L. M. High-Performance, Stretchable, Wire-Shaped Supercapacitors. *Angew. Chem., Int. Ed.* **2015**, *127*, 618−622.

(9) Lee, J.; Kim, W.; Kim, W. Stretchable Carbon Nanotube/Ion-Gel Supercapacitors with High Durability Realized through Interfacial Microroughness. *ACS Appl. Mater. Interfaces* **2014**, *6*, 13578−13586.

(10) Hong, S. Y.; Yoon, J.; Jin, S. W.; Lim, Y.; Lee, S. J.; Zi, G.; Ha, J. S. High-Density, Stretchable, All-Solid-State Microsupercapacitor Arrays. *ACS Nano* **2014**, *8*, 8844−8855.

(11) Yu, P.; Zhao, X.; Huang, Z.; Li, Y.; Zhang, Q. Free-standing Three-dimensional Graphene and Polyaniline Nanowire Arrays Hybrid Foams for High-performance Flexible and Lightweight Supercapacitors. *J. Mater. Chem. A* **2014**, *2*, 14413−14420.

DOI: 10.1021/acsami.5b03148
ACS Appl. Mater. Interfaces 2015, 7, 15303−15313

(12) Zhao, C.; Wang, C. Y.; Yue, Z. L.; Shu, K. W.; Wallace, G. G. Intrinsically Stretchable Supercapacitors Composed of Polypyrrole Electrodes and Highly Stretchable Gel Electrolyte. *ACS Appl. Mater. Interfaces* **2013**, *5*, 9008−9014.
(13) Wu, H.; Shevlin, S. A.; Meng, Q.; Guo, W.; Meng, Y.; Lu, K.; Wei, Z.; Guo, Z. Flexible and Binder-Free Organic Cathode for High-Performance Lithium-Ion Batteries. *Adv. Mater.* **2014**, *26*, 3338−3343.
(14) Park, M. H.; Noh, M.; Lee, S.; Ko, M.; Chae, S.; Sim, S.; Choi, S.; Kim, H.; Nam, H.; Park, S.; Cho, J. Flexible High-Energy Li-Ion Batteries with Fast-Charging Capability. *Nano Lett.* **2014**, *14*, 4083−4089.
(15) Sun, L.; Li, M.; Jiang, Y.; Kong, W.; Jiang, K.; Wang, J.; Fan, S. Sulfur Nanocrystals Confined in Carbon Nanotube Network As a Binder-Free Electrode for High-Performance Lithium Sulfur Batteries. *Nano Lett.* **2014**, *14*, 4044−4049.
(16) Zheng, C.; To, J. W. F.; Chao, W.; Zhenda, L.; Nan, L.; Chortos, A.; Lijia, P.; Fei, W.; Yi, C.; Zhenan, B. A Three-Dimensionally Interconnected Carbon Nanotube-Conducting Polymer Hydrogel Network for High-Performance Flexible Battery Electrodes. *Adv. Energy Mater.* **2014**, *4*, 1400207.
(17) Park, J.; Park, M.; Nam, G.; Lee, J. S.; Cho, J. All-Solid-State Cable-Type Flexible Zinc-Air Battery. *Adv. Mater.* **2015**, *27*, 1396−1401.
(18) Kang, D. J.; Cho, H. H.; Lee, I.; Kim, K. H.; Kim, H. J.; Liao, K.; Kim, T. S.; Kim, B. J. Enhancing Mechanical Properties of Highly Efficient Polymer Solar Cells Using Size-Tuned Polymer Nanoparticles. *ACS Appl. Mater. Interfaces* **2015**, *7*, 2668−2676.
(19) Kavan, L.; Liska, P.; Zakeeruddin, S. M.; Gratzel, M. Optically Transparent FTO-Free Cathode for Dye-Sensitized Solar Cells. *ACS Appl. Mater. Interfaces* **2014**, *6*, 22343−22350.
(20) Lee, S. M.; Biswas, R.; Li, W. G.; Kang, D.; Chan, L.; Yoon, J. Printable Nanostructured Silicon Solar Cells for High-Performance, Large-Area Flexible Photovoltaics. *ACS Nano* **2014**, *8*, 10507−10516.
(21) Roy-Mayhew, J. D.; Bozym, D. J.; Punckt, C.; Aksay, I. A. Functionalized Graphene as a Catalytic Counter Electrode in Dye-Sensitized Solar Cells. *ACS Nano* **2010**, *4*, 6203−6211.
(22) Li, K.; Zhen, H. Y.; Niu, L. Y.; Fang, X.; Zhang, Y. K.; Guo, R. S.; Yu, Y.; Yan, F.; Li, H. F.; Zheng, Z. J. Full-Solution Processed Flexible Organic Solar Cells Using Low-Cost Printable Copper Electrodes. *Adv. Mater.* **2014**, *26*, 7271−7278.
(23) Foo, C. Y.; Sumboja, A.; Tan, D. J. H.; Wang, J.; Lee, P. S. Flexible and Highly Scalable V_2O_5-rGO Electrodes in an Organic Electrolyte for Supercapacitor Devices. *Adv. Energy Mater.* **2014**, *4*, 1400236.
(24) Su, Z.; Yang, C.; Xie, B.; Lin, Z.; Zhang, Z.; Liu, J.; Li, B.; Kang, F.; Wong, C. P. Scalable Fabrication of MnO_2 Nanostructure Deposited on Free-standing Ni Nanocone Arrays for Ultrathin, Flexible, High-performance Micro-supercapacitort. *Energy Environ. Sci.* **2014**, *7*, 2652−2659.
(25) Saricilar, S.; Antiohos, D.; Shu, K. W.; Whitten, P. G.; Wagner, K.; Wang, C. Y.; Wallace, G. G. High Strain Stretchable Solid Electrolytes. *Electrochem. Commun.* **2013**, *32*, 47−50.
(26) Li, X.; Gu, T. L.; Wei, B. Q. Dynamic and Galvanic Stability of Stretchable Supercapacitors. *Nano Lett.* **2012**, *12*, 6366−6371.
(27) Yang, Y.; Li, L.; Ruan, G. D.; Fei, H. L.; Xiang, C. S.; Fan, X. J.; Tour, J. M. Hydrothermally Formed Three-Dimensional Nanoporous $Ni(OH)_2$ Thin-Film Supercapacitors. *ACS Nano* **2014**, *8*, 9622−9628.
(28) Long, C. L.; Qi, D. P.; Wei, T.; Yan, J.; Jiang, L. L.; Fan, Z. J. Nitrogen-Doped Carbon Networks for High Energy Density Supercapacitors Derived from Polyaniline Coated Bacterial Cellulose. *Adv. Funct. Mater.* **2014**, *24*, 3953−3961.
(29) Tang, Q. Q.; Wang, W. Q.; Wang, G. C. The Perfect Matching Between the Low-cost Fe_2O_3 Nanowire Anode and the NiO Nanoflake Cathode Significantly Enhances the Energy Density of Asymmetric Supercapacitors. *J. Mater. Chem. A* **2015**, *3*, 6662−6670.
(30) Yan, J.; Fan, Z.; Sun, W.; Ning, G.; Wei, T.; Zhang, Q.; Zhang, R.; Zhi, L.; Wei, F. Advanced Asymmetric Supercapacitors Based on $Ni(OH)_2$/Graphene and Porous Graphene Electrodes with High Energy Density. *Adv. Funct. Mater.* **2012**, *22*, 2632−2641.
(31) Fan, Z.; Yan, J.; Wei, T.; Zhi, L.; Ning, G.; Li, T.; Wei, F. Asymmetric Supercapacitors Based on Graphene/MnO_2 and Activated Carbon Nanofiber Electrodes with High Power and Energy Density. *Adv. Funct. Mater.* **2011**, *21*, 2366−2375.
(32) Khomenko, V.; Raymundo-Pinero, E.; Beguin, F. Optimisation of an Asymmetric Manganese Oxide/Activated Carbon Capacitor Working at 2 V in Aqueous Medium. *J. Power Sources* **2006**, *153*, 183−190.
(33) Liu, J. L.; Zhang, L. L.; Wu, H. B.; Lin, J. Y.; Shen, Z. X.; Lou, X. W. High-performance flexible asymmetric supercapacitors based on a new graphene foam/carbon nanotube hybrid film. *Energy Environ. Sci.* **2014**, *7*, 3709−3719.
(34) Niu, Z. Q.; Dong, H. B.; Zhu, B. W.; Li, J. Z.; Hng, H. H.; Zhou, W. Y.; Chen, X. D.; Xie, S. S. Highly Stretchable, Integrated Supercapacitors Based on Single-Walled Carbon Nanotube Films with Continuous Reticulate Architecture. *Adv. Mater.* **2013**, *25*, 1058−1064.
(35) Meng, F.; Ding, Y. Sub-micrometer-thick All-solid-state Supercapacitors with High Power and Energy Densities. *Adv. Mater.* **2011**, *23*, 4098−4102.
(36) Meng, C.; Liu, C.; Chen, L.; Hu, C.; Fan, S. Highly Flexible and All-Solid-State Paperlike Polymer Supercapacitors. *Nano Lett.* **2010**, *10*, 4025−4031.
(37) Haraguchi, K.; Takehisa, T. Nanocomposite hydrogels: A Unique Organic-inorganic Network Structure with Extraordinary Mechanical, Optical, and Swelling/de-swelling Properties. *Adv. Mater.* **2002**, *14*, 1120−1124.
(38) Schexnailder, P.; Schmidt, G. Nanocomposite Polymer Hydrogels. *Colloid Polym. Sci.* **2009**, *287*, 1−11.
(39) Jia, X.; Li, Y. F.; Cheng, Q.; Zhang, S. J.; Zhang, B. Preparation and Properties of Poly(vinyl alcohol)/silica Nanocomposites Derived from Copolymerization of Vinyl Silica Nanoparticles and Vinyl Acetate. *Eur. Polym. J.* **2007**, *43*, 1123−1131.
(40) Lin, W. C.; Fan, W.; Marcellan, A.; Hourdet, D.; Creton, C. Large Strain and Fracture Properties of Poly(dimethylacrylamide)/Silica Hybrid Hydrogels. *Macromolecules* **2010**, *43*, 2554−2563.
(41) Lin, J. B.; Chen, H. L.; Ji, Y.; Zhang, Y. Functionally Modified Monodisperse Core-Shell Silica Nanoparticles: Silane Coupling Agent as Capping and Size Tuning Agent. *Colloids Surf., A* **2012**, *411*, 111−121.
(42) Marini, M.; Pourabbas, B.; Pilati, F.; Fabbri, P. Functionally Modified Core-shell Silica Nanoparticles by One-pot Synthesis. *Colloids Surf., A* **2008**, *317*, 473−481.
(43) Stepniak, I.; Ciszewski, A. Electrochemical Characteristics of a New Electric Double Layer Capacitor with Acidic Polymer Hydrogel Electrolyte. *Electrochim. Acta* **2011**, *56*, 2477−2482.
(44) Hao, G. P.; Hippauf, F.; Oschatz, M.; Wisser, F. M.; Leifert, A.; Nickel, W.; Mohamed-Noriega, N.; Zheng, Z.; Kaskel, S. Stretchable and Semitransparent Conductive Hybrid Hydrogels for Flexible Supercapacitors. *ACS Nano* **2014**, *8*, 7138−7146.
(45) Wang, Q.; Hou, R.; Cheng, Y.; Fu, J. Super-tough Double-network Hydrogels Reinforced by Covalently Compositing with Silica-nanoparticles. *Soft Matter* **2012**, *8*, 6048−6056.
(46) Carlsson, L.; Rose, S.; Hourdet, D.; Marcellan, A. Nano-hybrid Self-crosslinked PDMA/silica hydrogels. *Soft Matter* **2010**, *6*, 3619−3631.
(47) Biswas, S.; Drzal, L. T. Multi layered Nanoarchitecture of Graphene Nanosheets and Polypyrrole Nanowires for High Performance Supercapacitor Electrodes. *Chem. Mater.* **2010**, *22*, 5667−5671.
(48) Yuan, L.; Yao, B.; Hu, B.; Huo, K.; Chen, W.; Zhou, J. Polypyrrole-coated Paper for Flexible Solid-state Energy Storage. *Energy Environ. Sci.* **2013**, *6*, 470−476.
(49) Yang, C. Y.; Shen, J. L.; Wang, C. Y.; Fei, H. J.; Bao, H.; Wang, G. C. All-solid-state Asymmetric Supercapacitor Based on Reduced Graphene Oxide/Carbon Nanotube and Carbon Fiber Paper/Polypyrrole Electrodes. *J. Mater. Chem. A* **2014**, *2*, 1458−1464.
(50) Chou, S. L.; Cheng, F. Y.; Chen, J. Electrodeposition Synthesis and Electrochemical Properties of Nanostructured Gamma-MnO_2 Films. *J. Power Sources* **2006**, *162*, 727−734.

DOI: 10.1021/acsami.5b03148
ACS Appl. Mater. Interfaces 2015, 7, 15303−15313

(51) Xie, Y. Z.; Liu, Y.; Zhao, Y. D.; Tsang, Y. H.; Lau, S. P.; Huang, H. T.; Chai, Y. Stretchable All-solid-state Supercapacitor with Wavy Shaped Polyaniline/Graphene Electrode. *J. Mater. Chem. A* **2014**, *2*, 9142−9149.
(52) Yu, M. H.; Zhang, Y. F.; Zeng, Y. X.; Balogun, M. S.; Mai, K. C.; Zhang, Z. S.; Lu, X. H.; Tong, Y. X. Water Surface Assisted Synthesis of Large-Scale Carbon Nanotube Film for High-Performance and Stretchable Supercapacitors. *Adv. Mater.* **2014**, *26*, 4724−4729.
(53) Yu, C. J.; Masarapu, C.; Rong, J. P.; Wei, B. Q.; Jiang, H. Q. Stretchable Supercapacitors Based on Buckled Single-Walled Carbon Nanotube Macrofilms. *Adv. Mater.* **2009**, *21*, 4793−4797.
(54) Yuan, L. Y.; Lu, X. H.; Xiao, X.; Zhai, T.; Dai, J. J.; Zhang, F. C.; Hu, B.; Wang, X.; Gong, L.; Chen, J.; Hu, C. G.; Tong, Y. X.; Zhou, J.; Wang, Z. L. Flexible Solid-State Supercapacitors Based on Carbon Nanoparticles/MnO_2 Nanorods Hybrid Structure. *ACS Nano* **2012**, *6*, 656−661.

DOI: 10.1021/acsami.5b03148
ACS Appl. Mater. Interfaces 2015, 7, 15303−15313